

## Observation of dust Coulomb clusters in a plasma trap

Wen-Tau Juan, Zen-Hong Huang, Ju-Wang Hsu, Yin-Ju Lai, and Lin I

*Department of Physics and Center for Complex Systems, National Central University, Chung-Li, Taiwan 320, Republic of China*

(Received 10 September 1998)

The formation of ordered quasi-two-dimensional Coulomb clusters of negatively charged dust particles with particle number  $N$ , from a few to 791 in a cylindrical plasma trap, are demonstrated. For small  $N$ , particles are alternately packed in concentric shells with periodically oscillating occupation numbers as  $N$  increases. The thermal induced collective excitations are dominated by the intershell angular motions. For large  $N$ , the large triangular core surrounded by a few outer circular shells appears and supports vortexlike excitations, which induce uniform and isotropic motions. The observed behaviors are generic and similar to the predictions by other more ideal models with the same symmetry. [S1063-651X(98)51412-2]

PACS number(s): 52.90.+z, 61.72.Ff, 82.70.Dd

The two-dimensional (2D) strongly coupled Coulomb cluster (SCCC) with small  $N$  is a mesoscopic nonlinear system with finite degrees of freedom, which exhibits rich microscopic structures and collective excitations. It is also a model system for the *classical atoms* proposed by J. J. Thomson with a small number of electrons embedded in a uniform neutralizing ion background, which generates parabolic confining potential [1]. The electrons on the liquid He surface and in the semiconductor quantum dot systems [2,3], and the flux lines in the superconductors and superfluids, are other examples sharing some similar features [4–6]. The recent theoretical studies indicate that the mutual Coulomb repulsion and the central confining field lead to the competition between the triangular lattice and circular shells associated with intrinsic defects for a 2D circular symmetric system. Regardless of the detailed interaction form, the generic packing behaviors, and anisotropic collective excitations under this symmetry have been predicted [7–10]. Nevertheless, to our knowledge, the structures and motions for the 2D SCCC's at different  $N$  have never been systematically studied in laboratories.

On the other hand, in a dusty plasma, the suspended dust particles can be strongly coupled due to their large charges ( $\sim 10^4$  electrons per  $\mu\text{m}$ -sized dust). As predicted by Ikezi [11], large volume dust crystals (with sub-mm lattice constant) and liquid states exhibiting interesting structures and motions have been directly observed at room temperature in recent experiments [12–17]. Quasi-2D hexagonal crystals can also be induced under the vertical ion flow [16,17]. Testing the formation and generic behaviors of dust clusters at small  $N$ , and the transition to large  $N$ , is certainly an interesting issue from the point of view of a classical Wigner crystal. In this work, using a cylindrical plasma trap that confines strongly charged  $\mu\text{m}$ -sized dust particles, we demonstrate the formation of quasi-2D SCCC's with  $N$  up to 791. Our findings of the shell structures, the alternate packing in different shells, the classical periodic table, the angular motion dominated excitations at small  $N$ , and the transition to the triangular lattice, with vortexlike excitations surrounded by the outer circular shells at large  $N$ , give the first direct experimental evidence of the theoretical predictions.

A cylindrical rf glow discharge system with 9-cm diameter and 4.5-cm height for our previous large volume dust

crystal experiment is modified for this experiment [12]. Instead of the large radius groove in our previous experiment, a hollow coaxial cylinder with 3-cm diameter and 1.5-cm height is put on the bottom electrode to confine dust particles in the weakly ionized glow discharge generated in Ar at a few hundred mTorr using a 14-MHz rf power system. Operating at very low rf power ( $<0.5$  W) makes the nonuniform dark space (i.e., the boundary layer), which is adjacent to the cylinder wall and supports outward radial space charge field, quite thick. It leaves a small glow region with uniform plasma density ( $n_e \sim 10^9 \text{ cm}^{-3}$ ), and a few mm diameter in the center of the trap. Introducing 5- $\mu\text{m}$ -diameter polystyrene particles to the glow sucks some electrons out and leaves an ion-rich background. Its space-charge field confines dust particles in the center uniform region. Decreasing rf power can increase the dark space width and, in turn, reduce the diameter of the cluster. Similarly to our previous experiments [5,6], ions flow downward from the glow above the cluster. It induces dipole interaction and causes the formation of vertical dust particle chains (each containing about 5–20 particles), even up to the cluster radial boundary. The chain only moves horizontally. The system can be treated as a quasi-2D system. The particle (chain) positions in the horizontal middle plane are monitored by a charge-coupled-device camera to investigate the 2D packing and motion. Figure 1 shows a few typical microimages of clusters up to large  $N$  with  $\frac{1}{30}$  sec exposure time.

For the system with small  $N$ , particles are located in concentric shells. Figure 2(a) shows a series of typical observed cluster configurations through the triangulation process as  $N$  increases. The state  $(N_1, N_2, N_3, \dots)$  has  $N_1, N_2, N_3, \dots$  particles in different shells from the center. For  $N=3, 4$ , and  $5$ , the polygons coaxial with the circular trap are formed. For  $N=6$ , a particle appears at the center of the pentagon to form a two-shell structure. Increasing  $N$  from 7 to 16 causes the alternative increase of  $N_2$  by one, first when  $\Delta N_1 = 5$  ( $\Delta N_i = N_{i+1} - N_i$ ), and then the increase of  $N_1$  by one until both shells are full (i.e.,  $N_1 = 5$  and  $N_2 = 11$ ). It suggests that the enlargement of one shell after adding one particle provides space for the adjacent shell to add the next particle.  $\Delta N_1$  fluctuates between 5 and 6 alternately. For  $N=17$ , the third shell appears. It forms a (1,5,11) structure. For the structure with three shells, similar filling processes are observed.

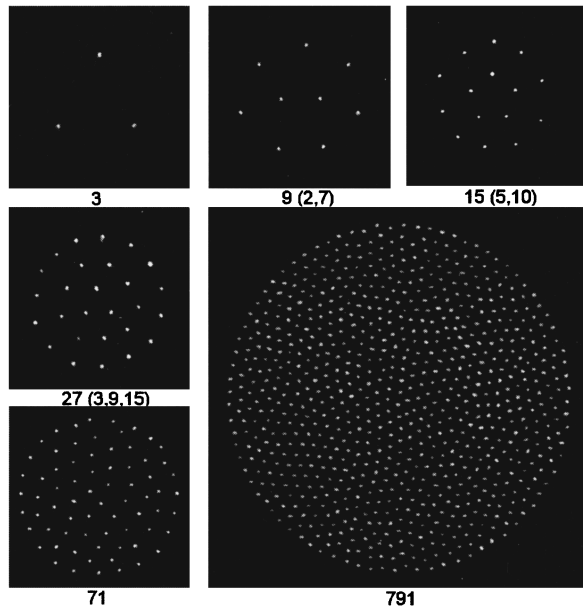


FIG. 1. Snapshots of the microimages of the typical cluster structure at different  $N$ . For displaying purposes, the scales are not the same for the pictures. The typical interparticle spacing is between 0.3 and 0.7 mm.

$(\Delta N_1, \Delta N_2)$  follows the periodic sequence of (5,6)-(6,5)-(6,6) as  $N$  increases one by one from 19 to 30. Figure 3 shows the alternate packing in different shells and the periodic oscillation of  $N_i$  as  $N$  increases. It corresponds to a classical periodic table. Unlike the *quantum atoms*, in which the addition of electrons is only allowed in the outer orbit, our packing sequence is generic and similar to the Monte Carlo simulation for 2D electrons in a parabolic confining well (i.e., a field generated by a uniform frozen ion background), except that  $N_i$  may deviate by one for  $N$  larger than 16 [7–9]. Many states predicted by the above model with similar energies such as (1,8), (1,8,13), (1,8,14), (3,9,13), etc. have also been observed in our experiment [7].

To understand the generic structures, three typical equilibrium states with different  $N_1$  are obtained from our 2D molecular dynamics (MD) simulation at zero temperature, with weak linear damping, a parabolic confining potential, and unshielded Coulomb repulsion [Fig. 2(b)]. They are quite similar to our experimental results. For an infinite 2D system, with mutual Coulomb repulsion, particles should sit at the triangular lattice sites shown in the background [9]. However, for a finite  $N$  system, the addition of the radial confining force tends to bend the lattice and form circular shell structures. The bending causes large strain energy especially when the radius of the curvature is small [9]. For structures with two, three, and four particles in the first shell, the particles of the second shell sit between a circular ring and a triangular lattice boundary. For example, the second shell is elliptical for the (2,8) state (Fig. 2). For the structures with three or four shells, only the outmost shell is more circular. The inner parts are more triangularlike to reduce strain energy. If some magic combinations for the inner shells such as (1,6), (2,8), (3,9), (4,10), (1,6,12), etc. can be reached, the inner part forms defect-free sixfold packing [7]. Besides the threefold defects along the outmost shell (a particle on the unbended edge of a triangular lattice should have

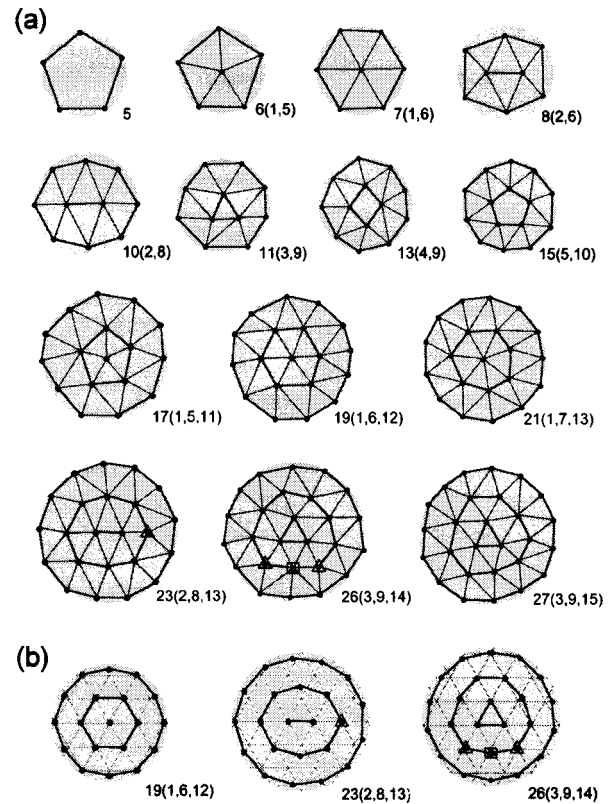


FIG. 2. (a) Typical snapshots of the triangulated cluster configurations observed at different  $N$ . The gray circles are drawn and triangulations are made for reference. (b) Three typical structures, from the 2D MD simulation with unshielded Coulomb repulsion, in a parabolic circular well. The triangular lattices are plotted as references to illustrate the bending from the central confining force. In (a) and (b), the small triangles and squares in a few images are the fivefold and sevenfold disclination defects, respectively.

four bonds), the unpaired intrinsic fivefold and sevenfold defects mainly stay around the second outmost shell if the outmost shell does not have six particles more than the adjacent shell [e.g., the 5-7-5 defects in the lower part of the (3,9,14) states in Figs. 2(a) and 2(b)].

This strongly coupled system supports many interesting thermally induced collective excitations. Under the shell

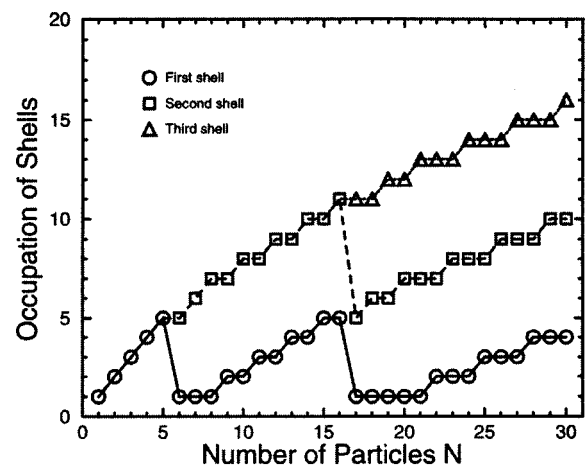


FIG. 3. Occupation number  $N_i$  vs  $N$ , showing the alternate packing to different shells and the periodic oscillation of  $N_i$ .

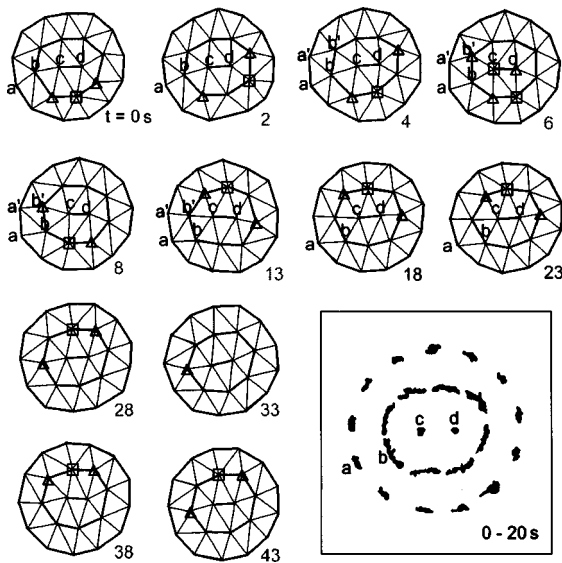


FIG. 4. (a) Evolution of the (2,8,13) state. The motion is dominated by the thermally induced intershell angular vibration and rotation as shown in the inset with 20 s exposure time, which make the system visit microstates with different associated fivefold (triangle) and sevenfold (square) defect combinations.

structure, induced by circular system symmetry, the collective intershell angular excitations predominate over other excitations, such as intrashell angular and radial motion, radial vibration of the whole cluster relative to the confining center, radial breathing, etc. [7,8,10]. It also makes the system access different states with different topologies. Figure 4 gives an experimental example of the time evolution of the (2,8,13) structure. The elongated trajectories and the different angular displacements for different shells manifest easier intershell angular motion than radial motion. The sequential snapshots with triangulation show the relative particle and defect (only the fivefold and sevenfold defects are marked) positions. The intershell and intrashell angular excitations associated with the slight radial vibration cause the generation, annihilation, circulation, and relative motions of the fivefold and sevenfold defects mainly around the (2,8) core. It accesses states with a few different topologies but similar energies. There are three stable or metastable defect configurations: single fivefold defect (at 33 s), a connected 5-7-5 defect cluster (e.g., at 0, 25, and 38 s), and a 5-7 defect pair with another fivefold defect separated by one dust particle (e.g., at 4, 8, 10, 28 s, etc.) around the second shell. Usually, the center two particles line up with their neighboring particles in the second shell. The 5 and 7 defects only temporally reach the center core during the switching of the alignment (e.g., from alignment  $a-b-c-d$  to  $a'-b'-c-d$  at 6 s). Namely, the small (2,8) core with full sixfold packing is quite robust. The intershell rotation is much harder to thermally excite than the intershell vibration between the first two shells.

As  $N$  becomes larger, the second-outermost shell also becomes piecewise circular, due to the lower bending energy at a larger radius [Figs. 5(a) and 5(b)]. The particles in the inner regions sit mainly in a more uniform and isotropic triangular lattice environment and feel a weaker boundary effect. The mean nearest neighbor separation  $a$ , measured from the first

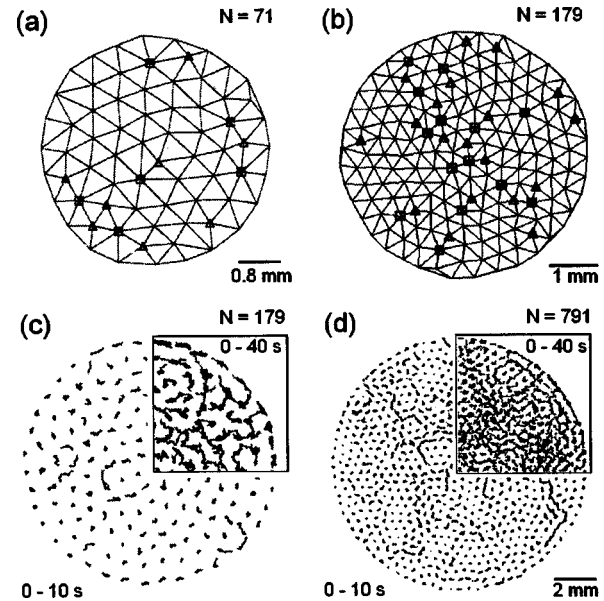


FIG. 5. (a) and (b). Triangulated configurations for the two typical large  $N$  states. The triangles and squares represent the fivefold and sevenfold defects, respectively. (c) and (d). Trajectories showing the vortex-like excitation. The insets with longer exposure time show that the isotropic random trajectories accumulated from the random-phase isotropic vortex excitations.

peak position of the pair correlation function, is uniform in the inner region, and only increases up to about 10% for radius  $0.7R < r < R$ . In the absence of the shell structure, the angular motion is no longer more preferred in the inner region. The vortex-type excitations, similar to our previous large-volume dusty plasma, are recovered [Figs. 5(c) and 5(d)] [5,6]. The excitations are quite uniform and isotropic, except for the outermost shell [see the insets of Figs. 5(c) and 5(d) for long time trajectories accumulated over many excitations]. In addition to the unpaired intrinsic threefold and fivefold defects, due to lattice bending in the outer circular shells, the vortex-type excitations also generate free dislocations with paired fivefold and sevenfold defects in the inner region [the state in Fig. 5(b) is hotter than in 5(a) due to the higher rf power, and shows more thermal defects]. The excitations also cause the competition between the straight lattice and the circular outer shells, and the temporal invasion of the straight lattice to various regions in outer shells [Figs. 5(a) and 5(b)].

Regardless of the complications, such as the Debye shielding from the unfrozen plasma background (the Debye length is of about the same order as the interdust distance) and the contribution from the particles along the vertical chains, the generic behaviors, such as the shell structures, alternate packing, periodic oscillation of  $N_i$ , and collective excitations observed, are quite similar to the predictions from the 2D models with unshielded Coulomb repulsions in a parabolic potential well [7–10]. It suggests that the circular system symmetry and mutual repulsion are the key factors determining the generic behaviors [9]. The detailed interaction forms have minor effects. Our recent MD simulations with different interaction forms also support this argument. For example, the harder core repulsion (e.g., Yukawa-type interaction) reduces  $\Delta N_i$  for the outer shells by one or two. The trend is reversed if the confining potential has additional

quadratic or higher order terms that make the potential steeper in the outer region [18].

In conclusion, we introduce our small plasma trap, which confines quasi-2D dust SCCC's with a wide range of  $N$ . For small  $N$ , particles are located in concentric shells. The competition between the central force and the mutual repulsion leads to the alternate packing in different shells and the periodic oscillation of  $N_i$  as  $N$  increases, and the formation of the circular outermost shell and the less circular inner shells. The angular motion dominated excitations under the shell structure make the system visit similar energy states with different defect topologies. The small core with magic packing number is robust and leaves the defects in the surround-

ing region. For large  $N$ , the number of circular shells surrounding the large triangular inner lattice slightly increases. Away from the boundary, the particle motions are uniform and isotropic due to the vortex-like excitations. Sharing the same symmetry, the generic behaviors of our system are similar to the predictions by models with uniform frozen neutralizing ions, although our neutralizing background has moving electrons and ions, and there are other complications from the vertical chains and the slightly stronger inward force, due to the slight excess of ions in the glow boundary.

This research was supported by the National Science Council of the Republic of China under Contract No. NSC-87-2118-M008-016.

- 
- [1] J. J. Thomson, *Philos. Mag.* **39**, 236 (1904).
  - [2] H. Ikezi, *Phys. Rev. Lett.* **42**, 1688 (1979); P. Leiderer, W. Ebner, and V. B. Shikin, *Surf. Sci.* **113**, 405 (1982).
  - [3] *Nanostructure Physics and Fabrication*, edited by M. A. Reed and W. P. Kirk (Academic, Boston, 1989).
  - [4] D. Reefman and H. B. Brom, *Physica C* **183**, 212 (1991).
  - [5] W. I. Glaberson and K. W. Schwartz, *Phys. Today* **40**(2), 54 (1987).
  - [6] Y. Kondo *et al.*, *Phys. Rev. Lett.* **68**, 3331 (1992).
  - [7] V. M. Bedanov and F. M. Peeters, *Phys. Rev. B* **49**, 2667 (1994).
  - [8] V. A. Schweigert and F. M. Peeters, *Phys. Rev. B* **51**, 7700 (1995).
  - [9] A. A. Koulakov and B. I. Shklovskii, *Phys. Rev. B* **55**, 9223 (1997).
  - [10] Y. E. Lozovik and V. A. Mandelshtam, *Phys. Lett. A* **145**, 269 (1990); **145**, 165 (1992); **145**, 465 (1992).
  - [11] H. Ikezi, *Phys. Fluids* **29**, 1764 (1986).
  - [12] J. H. Chu and Lin I, *Phys. Rev. Lett.* **72**, 4009 (1994).
  - [13] Y. Hayashi and K. Tachibana, *Jpn. J. Appl. Phys., Part 1* **33**, 804 (1994).
  - [14] G. E. Thomas *et al.*, *Phys. Rev. Lett.* **73**, 652 (1994).
  - [15] A. Melzer, T. Trottenberg, and A. Piel, *Phys. Lett. A* **191**, 301 (1994).
  - [16] Lin I, W. T. Juan, and C. H. Chiang, *Science* **272**, 1626 (1996).
  - [17] C. H. Chiang and Lin I, *Phys. Rev. Lett.* **77**, 647 (1996); W. T. Juan and Lin I, *ibid.* **80**, 3073 (1996).
  - [18] Y. J. Lai, W. T. Juan, and Lin I (unpublished).